GEOCHEMISTRY

Constraining the rate of oceanic deoxygenation leading up to a Cretaceous Oceanic Anoxic Event (OAE-2: ~94 Ma)

Chadlin M. Ostrander,[1,2,3]* Jeremy D. Owens,[2,3,4] Sune G. Nielsen[2,3]

Copyright © 2017
The Authors, some
rights reserved;
exclusive licensee
American Association
for the Advancement
of Science. No claim to
original U.S. Government
Works. Distributed
under a Creative
Commons Attribution
NonCommercial
License 4.0 (CC BY-NC).

The rates of marine deoxygenation leading to Cretaceous Oceanic Anoxic Events are poorly recognized and constrained. If increases in primary productivity are the primary driver of these episodes, progressive oxygen loss from global waters should predate enhanced carbon burial in underlying sediments—the diagnostic Oceanic Anoxic Event relic. Thallium isotope analysis of organic-rich black shales from Demerara Rise across Oceanic Anoxic Event 2 reveals evidence of expanded sediment-water interface deoxygenation ~43 ± 11 thousand years before the globally recognized carbon cycle perturbation. This evidence for rapid oxygen loss leading to an extreme ancient climatic event has timely implications for the modern ocean, which is already experiencing large-scale deoxygenation.

INTRODUCTION

Anthropogenic forcing of the ocean-atmosphere system necessitates an understanding of Oceanic Anoxic Events (OAEs) and the associated time scales and mechanisms of initiation to predict potential future marine deoxygenation (*1*). The cause of OAE-2, which occurred at the Cenomanian-Turonian boundary [~94 Ma (million years ago)], has been attributed to various combinations of increased surface temperatures (*2*), sea level rise (*3*), nutrient trapping (*4*), and pulses of magmatic activity (*5*–*7*)—all of which are likely to increase primary productivity (*7*). In the modern predominantly oxic ocean, primary productivity in the euphotic zone produces excess organic carbon that subsequently sinks and is remineralized to CO_2 by heterotrophic bacteria, in the process consuming free oxygen. Thus, increases in primary productivity are accompanied by increases in oxygen consumption and should lead to a progressive expansion in anoxic portions of the ocean (*8*). Recent advances place coarse temporal constraints on select OAE-2 trigger mechanisms (*9*–*11*) and provide evidence for this gradual marine deoxygenation (*12*–*16*), but the timing of the transition from widespread ocean oxygenation before OAE-2 to the peak of ocean deoxygenation remains effectively unconstrained. Uncertainty surrounding the exact duration of OAE-2—and thus also surrounding the timing of what is going on before and during the event—adds further complications, with recent estimates ranging from ~450 to 700 ky (thousand years) (*17*–*19*).

The massive burial of organic carbon during OAE-2 [perhaps 1.4 to 1.6 times that of the steady-state modern ocean (*14*, *20*)], which caused the observed carbon isotope excursion (*2*, *5*), must be linked to changes in redox conditions even when considering caveats from sedimentation rate changes (*21*, *22*). Manganese (Mn) oxides are ubiquitous in sediments deposited below an oxygenated water column but are absent under anoxic or euxinic conditions, because quantitative chemical reduction of insoluble Mn (IV) to more soluble Mn (II) and Mn (III) occurs when oxygen is essentially removed from the water in contact with the sediment (*23*). Attempts to directly track perturbations in both local and global Mn oxide burial have been proven difficult because of numerous factors, but primarily because Mn budgets in ancient marine sediments are often perturbed by postdepositional processes (*24*).

Thallium (Tl) strongly adsorbs to Mn oxides during their precipitation with a large positive isotope fractionation factor, rendering seawater isotopically light (*25*, *26*). Global Mn oxide precipitation is the primary control of the marine Tl isotope composition on time scales shorter than ~5 million years (*27*), and the modern marine residence time of Tl is ~18.5 ky (*28*). Therefore, reconstructions of the Tl isotope composition of seawater for short-term events, such as OAEs, should provide evidence of perturbations in Mn oxide precipitation. Recent work shows that, because Tl is quantitatively removed from seawater under euxinic conditions, sediments underlying these environments faithfully record the Tl isotope composition of overlying waters (*29*). As long as the euxinic setting is well connected to the open ocean (for example, Cariacao Basin, Venezuela), sediments in these locations record the global seawater value. Thus, ancient euxinic sediments are an archive capable of tracking changes in the global Mn oxide burial flux in cases where the overlying water column was well connected to open ocean seawater.

Here, we present Tl isotope compositions of organic-rich euxinic black shales before, during, and after OAE-2 that were recovered from ODP (Ocean Drilling Program) Site 1258 located on Demerara Rise in the Atlantic Ocean (table S1) (*30*). The stratigraphy and temporal framework of cores from Site 1258 sampled for this study are well constrained (see the Supplementary Materials for more details). The macroscopic view of the entire section has been shown to record local euxinic conditions based on Fe speciation (*15*) while, at the same time, being relatively well connected with the open ocean because of its paleogeographic location (fig. S1) (*30*). These observations show that samples from ODP Site 1258 are ideal for reconstructing changes in Mn oxide burial before, during, and after OAE-2 using Tl isotopes.

RESULTS

Before the event, Tl isotope compositions are slightly heavier than modern seawater values (ε^{205}Tl = −6) (*31*, *32*), averaging ε^{205}Tl ~ −4.5 and believed to represent connection to well-oxygenated global ocean (Fig. 1A; implications for this value are discussed in the Supplementary Materials). Most markedly, a distinct positive shift to ε^{205}Tl ~ −2.5 occurs before the onset of OAE-2 and is maintained until slightly before the

---

[1]School of Earth and Space Exploration, Arizona State University, Tempe, AZ 85287, USA. [2]NIRVANA (Non-traditional Isotope Research on Various Advanced Novel Applications) Laboratories, Woods Hole Oceanographic Institution, Woods Hole, MA 02543, USA. [3]Department of Geology and Geophysics, Woods Hole Oceanographic Institution, Woods Hole, MA 02543, USA. [4]Department of Earth, Ocean and Atmospheric Science, National High Magnetic Field Laboratory, Tallahassee, FL 32306, USA.
*Corresponding author. Email: cmostran@asu.edu

termination of the event, where Tl isotopes start recovering toward lighter values of ε^{205}Tl ~ −3. Low-resolution black shale analysis before and during OAE-2 from a second basin (Furlo, Marche-Umbria, Italy) reveals nearly identical values to Site 1258 both before and during enhanced organic carbon burial (fig. S2), suggesting that these two records faithfully record the global ocean Tl isotope composition with little or no significant basinal heterogeneity or restriction affecting Tl isotopes in these two locations.

DISCUSSION

We conclude that the positive Tl isotope excursion reflects diminished global Tl scavenging by Mn oxides due to an expansion of areas in the ocean with minimal to no oxygen at the sediment-water interface. The Tl isotope excursion commences significantly before the carbon isotope excursion at Site 1258 (Fig. 1B) (*33*). Using a linear sedimentation rate extrapolated from the OAE, and assuming that the duration of OAE-2 was 600 ky, we calculate a time lag of ~43 ± 11 ky between the initiation of the Tl and C isotope excursion (see the Supplementary Materials). Therefore, our data imply that deoxygenation of the sediment-water interface (as indicated by Tl isotopes) was initiated ~43 ± 11 ky before expansion of global euxinia, as indicated by C and S isotope systematics (*14*). The 600-ky duration for OAE-2 used here is also the value used in recent attempts to constrain the timing of possible OAE-2 trigger mechanisms (*10*, *11*), guided by the GSSP (Global Boundary Stratotype Section and Point) time scale and estimates from multiple sites (*17*, *18*). If the duration of OAE-2 was actually shorter or longer than the 600 ky assumed here, then our estimate of ~43 ± 11 ky is too long or too short, respectively.

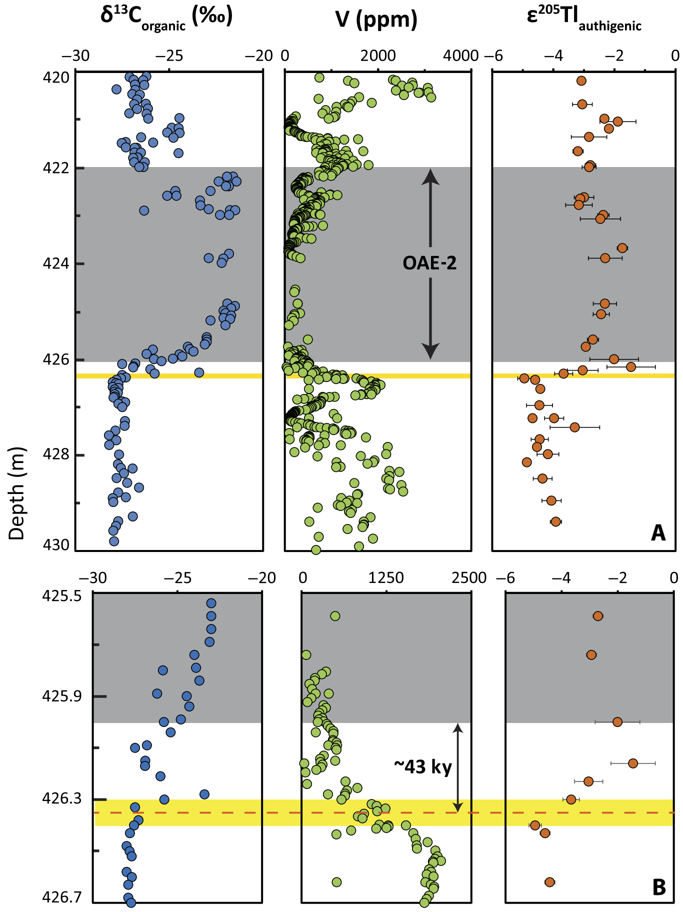

Fig. 1. Geochemical profile of ODP Site 1258 from Demerara Rise. (**A**) Spliced section analyzed for this study. OAE-2 is identified by the area in gray, as delineated by the carbon isotope excursion (*33*), and the shaded yellow region represents the onset of the Tl isotope shift. Vanadium concentrations are from previous studies (*15*, *37*). (**B**) Zoomed-in view of the profile immediately preceding OAE-2, highlighting the timing between the Tl isotope shift and disturbance of the global C cycle. Error bars represent 2-SD uncertainty of multiple sample analyses or the long-term reproducibility of SCO-1, whichever is greater.

The decrease in Mn oxide burial before OAE-2 can be modeled using a previously used isotope mass balance model (*27*). Although euxinic sediments accumulate significant Tl concentrations and, therefore, may constitute a significant Tl sink when marine euxinia expands, anoxic sediments deposited underneath oxygen minimum zones (OMZs) appear to have essentially little to no Tl enrichment (*34*). Therefore, we can treat the initial deoxygenation before OAE-2 where marine euxinia was yet to expand in terms of the same inputs and outputs that govern the modern marine Tl isotope reservoir. The shift from $\varepsilon^{205}\text{Tl} = -4.5$ to −2.5 before OAE-2 can be accounted for if Mn oxide output fluxes decreased by ~40 to 80%, depending on the Tl isotope fractionation factor between seawater and Mn oxides (see Fig. 2 and the Supplementary Materials for further details).

To our knowledge, this is the first study to track global perturbations in Mn oxide burial leading to a major climatic event. We can use these changes in Mn oxide burial as a direct measure of the seafloor area affected by anoxia. For this study, we refer to sediments being deposited beneath a sediment-water interface with oxygen concentrations close to 0, at least long enough to prevent Mn oxide burial, as anoxic. Thus, we can convert the ~40 to 80% change in Mn oxide burial flux into the area of anoxic seafloor by assuming that the areal extent of Mn oxide deposition was the primary control of Mn oxide burial fluxes over short time scales. Therefore, our model suggests that over a period of ~43 ± 11 ky, the area of anoxic seafloor expanded by 40 to 80%, or at a rate of ~2.2×10^3 to 7.5×10^3 km^2/year, substituting for previously oxygenated portions of the sediment-water interface (see the Supplementary Materials). If these oxygen depletions primarily manifested themselves via expansion of areas similar to modern OMZs, then more

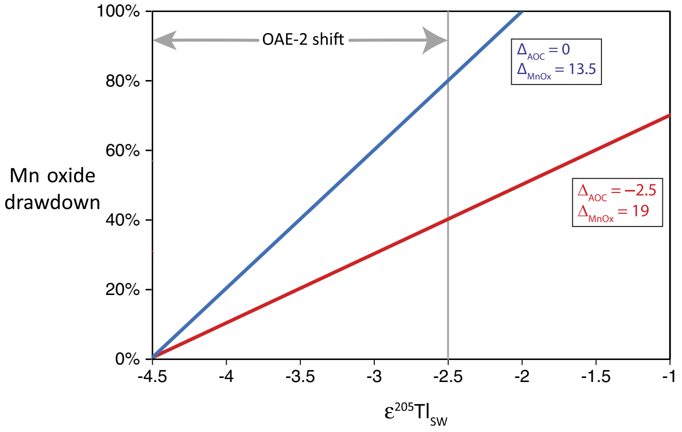

Fig. 2. The modeled decrease in Mn oxide burial associated with the Tl isotope shift from this study. Percentage of Mn oxide drawdown is calculated using the range of reported values for Tl isotope fractionation during incorporation into altered oceanic crust (AOC) and Mn oxides (MnOx) (inset boxes) (*28*). This yields a range of drawdown between 40 and 80% during OAE-2 (see the Supplementary Materials).

than the entire continental shelf and upper slope [~16% of the modern seafloor area (*35*), although this area was likely larger during OAE-2 because of higher sea levels (*3*)] would have been affected by periodic oxygen depletion. However, deoxygenation over large areas of the deep ocean (that is, abyssal, oligotrophic regions) is very difficult to maintain under a well-oxygenated atmosphere (*36*). Therefore, it is more likely that anoxic expansion was closer to our lower estimate of 40% (see the Supplementary Materials for further discussion).

By combining our results with previously published time constraints for possible OAE-2 trigger mechanisms and subsequent marine response, a clearer picture of pre–OAE-2 conditions materializes (Fig. 3). We assume that these conditions occurred over a backdrop of elevated surface temperatures (*2*) and paleocontinental arrangement (*4*) during the mid-Cretaceous that were conducive to enhanced nutrient delivery and sequestration, respectively. The initial trigger mechanism of changes in oceanic (de)oxygenation was likely the onset of large igneous province (LIP) activity, which occurred ~200 ky before OAE-2 (*10*). The initiation of LIP activity likely enhanced nutrient delivery to the ocean even further and could have primed Cretaceous oceans for oxygen loss. Global oxygen loss from the water column becomes evident at ODP Site 1258 ~59 ky before OAE-2, when global drawdown of the oceanic vanadium reservoir begins (see the Supplementary Materials) (*15*, *37*). Vanadium drawdown from the water column is probably linked to the V^{5+}–V^{4+} redox couple because of the more efficient incorporation of reduced V into organic matter (*38*). Reduction of V^{5+} to V^{4+} does not require complete removal of oxygen from seawater (*23*), and therefore, V drawdown is expected to precede significant reduction in Mn oxide burial, consistent with the Tl isotopic shift postdating V drawdown by ~16 ky (Fig. 1). The difference in timing between V concentrations and Tl isotopes is unlikely to be due to different marine reservoir effects because Tl has a shorter residence time than V [~18.5 ky (*28*) versus ~100 ky (*39*)], and thus, global perturbation of marine Tl would precede that of V should this be the case. It was not until unradiogenic Os isotope values were delivered to sediments worldwide, ~50 ky before OAE-2, likely because of the onset of the main LIP activity (*10*, *11*), that deoxygenation became severe enough to greatly affect global Mn oxide burial, as delineated by the observed Tl isotope excursion (Fig. 1). It is likely that the dissolution of Mn oxides at this time liberated not only Mn from the oxic sediments (*40*) but also many adsorbed trace metals including Tl and Mo, which is recorded in euxinic Demerara Rise sediments, as Mo concentrations briefly exceeded 600 parts per million (*15*, *37*) and the Tl isotope excursion reached values heavier than oceanic inputs [ε^{205}Tl = −1.5 ± 0.8 at 426.16 mcd (meters composite depth)]. It was not until a significant area of productive, marginal portions of the ocean was affected by oxygen depletion that enhanced global pyrite and carbon burial commenced in earnest, marking the onset of OAE-2 (*14*). The outlined sequence of events is in agreement with models that invoke enhanced primary productivity as the main mechanism responsible for inducing the OAE (*2*, *8*, *10*, *11*, *36*).

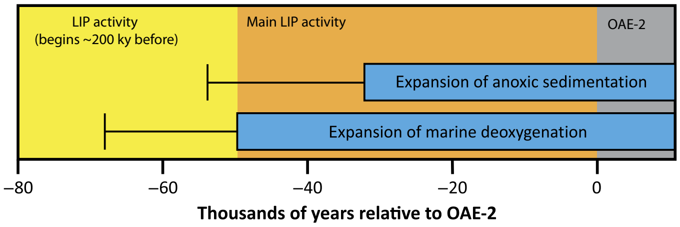

Fig. 3. Temporal constraints for pre–OAE-2 trigger mechanisms and changes in oceanic redox. All estimates are derived from constant sedimentation rates for ODP Site 1258 and depend on an estimate for the duration of OAE-2 of 600 ky (see the Supplementary Materials). LIP activity time constraints are from Os isotope data (*10*, *11*). The expanded marine deoxygenation estimate is based on the drawdown of the oceanic V reservoir (*15*, *37*), and the expansion of anoxic sedimentation estimate comes from this study (see the Supplementary Materials for more information). Error bars represent the difference between upper and lower time estimates, as explained in the Supplementary Materials.

In addition to the pre-OAE lag between the Tl and C isotope excursions, it is also significant that the recovery of Tl isotopes appears to be significantly slower than that of C isotopes (Fig. 1). In principle, this implies that Mn oxide burial, and thereby the global extent of anoxia, did not recover significantly even after organic carbon burial had largely diminished to pre-OAE levels. This post-OAE decoupling of the two isotope systems could imply that although overall organic matter burial declined, productivity was still sufficiently high to maintain the consumption of any oxygen that might have been subducted into the deep ocean through ocean circulation. Such a conclusion is supported by the fact that Os isotope values do not return to pre-event radiogenic values in most of the studied sites (*10*, *11*), which may indicate that significant LIP activity continued even after the recovery of C isotopes. In this case, the nutrient supply that fueled the initial increase in primary productivity could have remained relatively high and possibly maintained the expanded state of global anoxia. Alternatively, it has been hypothesized that the termination of increased carbon burial during OAE-2 was due to the drawdown of bioessential trace metals from seawater (*15*), which might have inhibited some parts of the carbon cycle and, therefore, reduced carbon burial even in the face of enhanced nutrient supply from LIP activity. Additionally, after the main OAE-2 event, a second positive C isotope excursion [between 421.19 and 420.98 mcd (Fig. 1)] and coeval drop in V concentrations are accompanied by a sudden positive Tl isotope excursion. These geochemical shifts are identical to those associated with the main OAE event, but the magnitudes are much smaller. Although this conclusion is speculative, this feature may imply a shorter-lived spike of deoxygenation and enhanced carbon burial that occurred shortly after OAE-2.

On the basis of our interpreted sequence of events leading up to OAE-2, the general marine response to increased nutrient supply, global warming, and sea level rise is expansion of oceanic anoxia without simultaneous expansion of ocean euxinia. Increased ocean deoxygenation is already apparent in the modern ocean, because marine O$_2$ has decreased by 2% over roughly the last half century (*41*), and recent models predict a continued loss of 0.5 to 3.5% over the next half century (*1*, *42*), which would result in huge expansions of ocean anoxia within the next few thousand years. Should anthropogenically induced oxygen loss occur at similar rates as in the period leading up to OAE-2, then the current area of seafloor hypoxia [currently ~764,000 km^2 (*43*)] would double in the next ~102 to 344 years, equivalent to an increase of ~2.2×10^4 to 7.5×10^4 km^2 of seafloor every decade—an easily detectable value. Localized oxygen loss is already apparent in the modern ocean (*1*, *41*, *42*), and the ability to observe more widespread perturbation seems realistic under currently projected carbon emissions. Without positive human intervention, ancient OAE studies are destined to become uncomfortably applicable in the not-so-distant future.

MATERIALS AND METHODS

Sample digestion

Previously powdered samples were digested using a technique modified from previous literature (*34*). Samples were first treated with 2 M HNO$_3$

to separate authigenic and detrital components, and the supernatant was isolated from the silicate residue. This partial dissolution was immediately followed by 1.5 hours of digestion at ~300°C and 100 bars in a high-pressure asher to help dissolve organic compounds. Following dissolution of the silicate residue in 1:1 concentrated HNO_3 and HF, both fractions were completely dissolved in 1 M HCl in preparation for ion exchange chromatography.

Tl purification

Thallium was isolated from a sample matrix using previously described anion exchange chromatography techniques (*31*, *44*). However, unlike previous studies, only one column was used during Tl purification. Testing of standards and samples showed that there was no difference in concentration or isotope composition between samples that had been processed through one or two columns (table S2).

Sample analysis

The Tl isotope compositions were determined at the Woods Hole Oceanographic Institution (WHOI) Plasma Mass Spectrometry Facility using a Thermo Finnigan Neptune multiple collector inductively coupled plasma mass spectrometer. Isotopic compositions are reported relative to the National Institute of Standards and Technology (NIST) 997 Tl metal in epsilon notation

$$\varepsilon^{205}\mathrm{Tl} = \left[\left(\varepsilon^{205/203}\mathrm{Tl}_{\mathrm{sample}}\right)/\left(\varepsilon^{205/203}\mathrm{Tl}_{\mathrm{NIST\ 997}}\right) - 1\right] \times 10^4$$

Previously described techniques that used both external normalization to NIST SRM (Standard Reference Materials) 981 Pb and standard-sample bracketing were applied for mass bias correction (*31*, *44*). Because of the quantitative yields of Tl from the column chemistry procedure, Tl concentrations were determined by monitoring the ^{205}Tl signal intensities of the samples during the isotopic measurements. A known quantity of NIST SRM 981 Pb was added to the sample Tl, and the measured ^{205}Tl/^{208}Pb ratios were then converted directly into Tl abundances. The U.S. Geological Survey (USGS) shale standard SCO-1 was processed and analyzed, with each sample set to monitor long-term precision and accuracy of our Tl isotope data (average calculated $\varepsilon^{205}\mathrm{Tl} = -2.64 \pm 0.24$; table S3), and was found to be better than most recent Tl isotope studies, which have 2-SD uncertainties of ~0.3 to 0.5 ε^{205}Tl units (*45*).

SUPPLEMENTARY MATERIALS

Supplementary material for this article is available at http://advances.sciencemag.org/cgi/content/full/3/8/e1701020/DC1
Supplementary Text
fig. S1. Paleogeographic locations of the sites analyzed in this study during the Cenomanian-Turonian boundary Anoxic Event (OAE-2: ~94 Ma).
fig. S2. Geochemical data from interbedded shales of the Furlo section in Central Italy.
fig. S3. Tl isotope composition of the authigenic fraction alongside that of the detrital fraction to show similarity.
table S1. Tl isotope and concentration data.
table S2. Reproducibility of Tl isotope composition with one column versus two columns.
table S3. Reproducibility of USGS shale standard SCO-1.
References (*46*–*50*)

REFERENCES AND NOTES

1. R. F. Keeling, A. Körtzinger, N. Gruber, Ocean deoxygenation in a warming world. *Annu. Rev. Mar. Sci.* **2**, 199–229 (2010).
2. S. O. Schlanger, H. C. Jenkyns, Cretaceous anoxic events: Causes and consequences. *Geol. Mijnbouw.* **55**, 179–184 (1976).
3. M. A. Arthur, S. O. Schlanger, H. C. Jenkyns, The Cenomanian/Turonian Oceanic Anoxic Event, II: Palaeoceanographic controls on organic matter production and preservation. *Spec. Publ. Geol. Soc. London* **26**, 401–420 (1987).
4. J. T. Alexandre, E. Tuenter, G. A. Henstra, K. J. van der Zwan, R. S. W. van de Wal, H. A. Dijkstra, P. L. de Boer, The mid-Cretaceous North Atlantic nutrient trap: Black shales and OAEs. *Paleoceanography* **25**, PA4201 (2010).
5. R. M. Leckie, T. J. Bralower, R. Cashman, Oceanic anoxic events and plankton evolution: Biotic response to tectonic forcing during the mid-Cretaceous. *Paleoceanography* **17**, 13-1–13-29 (2002).
6. D. D. Adams, M. T. Hurtgen, B. B. Sageman, Volcanic triggering of a biogeochemical cascade during Oceanic Anoxic Event 2. *Nat. Geosci.* **3**, 201–204 (2010).
7. J. D. Owens, T. W. Lyons, X. Li, K. G. Macleod, G. Gordon, M. M. M. Kuypers, A. D. Anbar, W. Kuhnt, S. Severmann, Iron isotope and trace metal records of iron cycling in the proto-North Atlantic during the Cenomanian-Turonian oceanic anoxic event (OAE-2). *Paleoceanography* **27**, PA3223 (2012).
8. K. M. Meyer, L. R. Kump, Oceanic euxinia in earth history: Causes and consequences. *Annu. Rev. Earth Planet. Sci.* **36**, 251–288 (2008).
9. S. C. Turgeon, R. A. Creaser, Cretaceous oceanic anoxic event 2 triggered by a massive magmatic episode. *Nature* **454**, 323–326 (2008).
10. A. D. C. Du Vivier, D. Selby, B. B. Sageman, I. Jarvis, D. R. Gröcke, S. Voigt, Marine ^{187}Os/^{188}Os isotope stratigraphy reveals interaction of volcanism and ocean circulation during Oceanic Anoxic Event 2. *Earth Planet. Sci. Lett.* **389**, 23–33 (2014).
11. A. D. C. Du Vivier, D. Selby, D. J. Condon, R. Takashima, H. Nishi, Pacific ^{187}Os/^{188}Os isotope chemistry and U–Pb geochronology: Synchroneity of global Os isotope change across OAE 2. *Earth Planet. Sci. Lett.* **428**, 204–216 (2015).
12. H. P. Mort, T. Adatte, K. B. Föllmi, G. Keller, P. Steinmann, V. Matera, Z. Berner, D. Stüben, Phosphorus and the roles of productivity and nutrient recycling during oceanic anoxic event 2. *Geology* **35**, 483–486 (2007).
13. Z. Lue, H. C. Jenkyns, R. E. M. Rickaby, Iodine to calcium ratios in marine carbonate as a paleo-redox proxy during oceanic anoxic events. *Geology* **38**, 1107–1110 (2010).
14. J. D. Owens, B. C. Gill, H. C. Jenkyns, S. M. Bates, S. Severmann, M. M. M. Kuypers, R. G. Woodfine, T. W. Lyons, Sulfur isotopes track the global extent and dynamics of euxinia during Cretaceous Oceanic Anoxic Event 2. *Proc. Natl. Acad. Sci. U.S.A.* **110**, 18407–18412 (2013).
15. J. D. Owens, C. T. Reinhard, M. Rohrssen, G. D. Love, T. W. Lyons, Empirical links between trace metal cycling and marine microbial ecology during a large perturbation to Earth's carbon cycle. *Earth Planet. Sci. Lett.* **449**, 407–417 (2016).
16. A. J. Dickson, H. C. Jenkyns, D. Porcelli, S. van den Boorn, E. Idiz, Basin-scale controls on the molybdenum-isotope composition of seawater during Oceanic Anoxic Event 2 (Late Cretaceous). *Geochim. Cosmochim. Acta* **178**, 291–306 (2016).
17. B. B. Sageman, S. R. Meyers, M. A. Arthur, Orbital time scale and new C-isotope record for Cenomanian-Turonian boundary stratotype. *Geology* **34**, 125–128 (2006).
18. S. R. Meyers, B. B. Sageman, M. A. Arthur, Obliquity forcing of organic matter accumulation during Oceanic Anoxic Event 2. *Paleoceanography* **27**, PA3212 (2012).
19. J. S. Eldrett, C. Ma, S. C. Bergman, B. Lutz, F. J. Gregory, P. Dodsworth, M. Phipps, P. Hardas, D. Minisini, A. Ozkan, J. Ramezani, S. A. Bowring, S. L. Kamo, K. Ferguson, C. Macaulay, A. E. Kelly, An astronomically calibrated stratigraphy of the Cenomanian-Turonian and earliest Coniacian from the Cretaceous Western Interior Seaway, USA: Implications for global chronostratigraphy. *Cretaceous Res.* **56**, 316–344 (2015).
20. L. R. Kump, M. A. Arthur, Interpreting carbon-isotope excursions: Carbonates and organic matter. *Chem. Geol.* **161**, 181–198 (1999).
21. D. E. Canfield, Factors influencing organic carbon preservation in marine sediments. *Chem. Geol.* **114**, 315–329 (1994).
22. H. E. Hartnett, R. G. Keil, J. I. Hedges, A. H. Devol, Influence of oxygen exposure time on organic carbon preservation in continental margin sediments. *Nature* **391**, 572–575 (1998).
23. E. L. Rue, G. J. Smith, G. A. Cutter, K. W. Bruland, The response of trace element redox couples to suboxic conditions in the water column. *Deep-Sea Res. I Oceanogr. Res. Pap.* **44**, 113–134 (1997).
24. D. J. Burdige, The biogeochemistry of manganese and iron reduction in marine sediments. *Earth Sci. Rev.* **35**, 249–284 (1993).
25. M. Rehkämper, M. Frank, J. R. Hein, D. Porcelli, A. N. Halliday, J. Ingri, V. Liebetrau, Thallium isotope variations in seawater and hydrogenetic, diagenetic, and hydrothermal ferromanganese deposits. *Earth Planet. Sci. Lett.* **197**, 65–81 (2002).
26. S. G. Nielsen, L. E. Wasylenki, M. Rehkämper, C. L. Peacock, Z. Xue, E. M. Moon, Towards an understanding of thallium isotope fractionation during adsorption to manganese oxides. *Geochim. Cosmochim. Acta* **117**, 252–265 (2013).
27. S. G. Nielsen, S. Mar-Gerrison, A. Gannoun, D. LaRowe, V. Klemm, A. N. Halliday, K. W. Burton, J. R. Hein, Thallium isotope evidence for a permanent increase in marine organic carbon export in the early Eocene. *Earth Planet. Sci. Lett.* **278**, 297–307 (2009).

28. S. G. Nielsen, M. Rehkämper, J. Prytulak, Investigation and application of thallium isotope fractionation. *Rev. Mineral. Geochem.* **82**, 759–798 (2017).
29. J. D. Owens, S. G. Nielsen, T. J. Horner, C. M. Ostrander, L. C. Peterson, Thallium-isotopic compositions of euxinic sediments as a proxy for global manganese-oxide burial. *Geochim. Cosmochim. Acta* 10.1016/j.gca.2017.06.041 (2017).
30. Shipboard Scientific Party, Site 1258. *Proc. Ocean Drill. Program: Initial Rep.* **207**, 1–117 (2004).
31. S. G. Nielsen, M. Rehkämper, J. A. Baker, A. N. Halliday, The precise and accurate determination of thallium isotope compositions and concentrations for water samples by MC-ICPMS. *Chem. Geol.* **204**, 109–124 (2004).
32. S. G. Nielsen, M. Rehkämper, D. A. H. Teagle, D. A. Butterfield, J. C. Alt, A. N. Halliday, Hydrothermal fluid fluxes calculated from the isotopic mass balance of thallium in the ocean crust. *Earth Planet. Sci. Lett.* **251**, 120–133 (2006).
33. J. Erbacher, O. Friedrich, P. A. Wilson, H. Birch, J. Mutterlose, Stable organic carbon isotope stratigraphy across Oceanic Anoxic Event 2 of Demerara Rise, western tropical Atlantic. *Geochem. Geophys. Geosyst.* **6**, Q06010 (2005).
34. S. G. Nielsen, M. Goff, S. P. Hesselbo, H. C. Jenkyns, D. E. LaRowe, C.-T. A. Lee, Thallium isotopes in early diagenetic pyrite—A paleoredox proxy? *Geochim. Cosmochim. Acta* **75**, 6690–6704 (2011).
35. H. W. Menard, S. M. Smith, Hypsometry of ocean basin provinces. *J. Geophys. Res.* **71**, 4305–4325 (1966).
36. H. C. Jenkyns, Geochemistry of oceanic anoxic events. *Geochem. Geophys. Geosyst.* **11**, Q03004 (2010).
37. A. Hetzel, M. E. Böttcher, U. G. Wortmann, H.-J. Brumsack, Paleo-redox conditions during OAE 2 reflected in Demerara Rise sediment geochemistry (ODP Leg 207). *Palaeogeogr. Palaeoclimatol. Palaeoecol.* **273**, 302–328 (2009).
38. M. D. Lewan, J. B. Maynard, Factors controlling enrichment of vanadium and nickel in the bitumen of organic sedimentary rocks. *Geochim. Cosmochim. Acta* **46**, 2547–2560 (1982).
39. J. L. Morford, S. Emerson, The geochemistry of redox sensitive trace metals in sediments. *Geochim. Cosmochim. Acta* **63**, 1735–1750 (1999).
40. H. C. Jenkyns, A. J. Dickson, M. Ruhl, S. H. J. M. van den Boorn, Basalt-seawater interaction, the Plenus Cold Event, enhanced weathering and geochemical change: Deconstructing OAE 2 (Cenomanian-Turonian, Late Cretaceous). *Sedimentology* **64**, 16–43 (2017).
41. S. Schmidtko, L. Stramma, M. Visbeck, Decline in global oceanic oxygen content during the past five decades. *Nature* **542**, 335–339 (2017).
42. M. C. Long, C. Deutsch, T. Ito, Finding forced trends in oceanic oxygen. *Global Biogeochem. Cycles* **30**, 381–397 (2016).
43. J. J. Holly, L. A. Levin, Global distribution of naturally occurring marine hypoxia on continental margins. *Deep Sea Res. I* **51**, 1159–1168 (2004).
44. M. Rehkämper, A. N. Halliday, The precise measurement of Tl isotopic compositions by MC-ICPMS: Applications to the analysis of geological materials and meteorites. *Geochim. Cosmochim. Acta* **63**, 935–944 (1999).
45. M. Kersten, T. Xiao, K. Kreissig, A. Brett, B. J. Coles, M. Rehkämper, Tracing anthropogenic thallium in soil using stable isotope compositions. *Environ. Sci. Technol.* **48**, 9030–9036 (2014).
46. J. D. Owens, T. W. Lyons, D. S. Hardisty, C. M. Lowery, Z. Lu, B. Lee, H. C. Jenkyns, Patterns of local and global redox variability during the Cenomanian-Turonian Boundary Event (Oceanic Anoxic Event 2) recorded in carbonates and shales from central Italy. *Sedimentology* **64**, 168–185 (2017).
47. S. G. Nielsen, M. Rehkämper, Thallium isotopes and their application to problems in earth and environmental science, in *Handbook of Environmental Isotope Geochemistry*, M. Baskaran Ed. (Springer, 2011), pp. 247–270.
48. W. W. Hay, J. L. Sloan II, C. N. Wold, Mass/age distribution and composition of sediments on the ocean floor and the global rate of sediment subduction. *J. Geophys. Res.* **93**, 14933–14940 (1988).
49. J. D. Milliman, Production and accumulation of calcium carbonate in the ocean: Budget of a nonsteady state. *Global Biogeochem. Cycles* **7**, 927–957 (1993).
50. C. R. Scotese, *Cretaceous Paleogeographic and Plate Tectonic Reconstructions*, vol. 2 of *The PALEOMAP Project PaleoAtlas for ArcGIS* (PALEOMAP Project, 2008).

Acknowledgments: We thank J. Blusztajn for his help with Tl isotope analyses at the WHOI Plasma Mass Spectrometry Facility and J. Sutton for his assistance in generating Tl isotope data from the Furlo section samples. **Funding:** We would like to acknowledge support from the NSF grant OCE 1434785 (to J.D.O. and S.G.N.), the NASA Exobiology grant NNX16AJ60G (to J.D.O. and S.G.N.), a WHOI Summer Student Fellowship (to C.M.O.), and an Agouron Postdoctoral Fellowship (to J.D.O.). This material is based on work supported by the NSF Graduate Research Fellowship Program under grant no. 026257-001. Any opinions, findings, and conclusions or recommendations expressed in this material are those of the authors and do not necessarily reflect the views of the NSF. **Author contributions:** J.D.O. and S.G.N. developed the project idea. C.M.O. performed Tl isotope and modeling analyses with contributions from J.D.O. and S.G.N. C.M.O. wrote the manuscript with significant contributions from J.D.O. and S.G.N. **Competing interests:** The authors declare that they have no competing interests. **Data and materials availability:** All data needed to evaluate the conclusions in the paper are present in the paper and/or the Supplementary Materials. Additional data related to this paper may be requested from the authors.

Submitted 28 March 2017
Accepted 11 July 2017
Published 9 August 2017
10.1126/sciadv.1701020

Citation: C. M. Ostrander, J. D. Owens, S. G. Nielsen, Constraining the rate of oceanic deoxygenation leading up to a Cretaceous Oceanic Anoxic Event (OAE-2: ~94 Ma). *Sci. Adv.* **3**, e1701020 (2017).

Science Advances

Constraining the rate of oceanic deoxygenation leading up to a Cretaceous Oceanic Anoxic Event (OAE-2: ~94 Ma)

Chadlin M. Ostrander, Jeremy D. Owens and Sune G. Nielsen

Sci Adv **3** (8), e1701020.
DOI: 10.1126/sciadv.1701020

ARTICLE TOOLS http://advances.sciencemag.org/content/3/8/e1701020

SUPPLEMENTARY MATERIALS http://advances.sciencemag.org/content/suppl/2017/08/07/3.8.e1701020.DC1

REFERENCES This article cites 46 articles, 5 of which you can access for free
http://advances.sciencemag.org/content/3/8/e1701020#BIBL

PERMISSIONS http://www.sciencemag.org/help/reprints-and-permissions

Use of this article is subject to the Terms of Service

Science Advances (ISSN 2375-2548) is published by the American Association for the Advancement of Science, 1200 New York Avenue NW, Washington, DC 20005. 2017 © The Authors, some rights reserved; exclusive licensee American Association for the Advancement of Science. No claim to original U.S. Government Works. The title *Science Advances* is a registered trademark of AAAS.